The Vertical Structure of Low-Frequency Motions in the Nearshore. Part II: Theory

THOMAS C. LIPPMANN

Department of Earth Sciences, Center for Coastal and Ocean Mapping, University of New Hampshire, Durham, New Hampshire

ANTHONY J. BOWEN

Department of Oceanography, Dalhousie University, Halifax, Nova Scotia, Canada

(Manuscript received 14 January 2016, in final form 21 September 2016)

ABSTRACT

Field observations from a vertical stack of two-component current meters obtained from the 1994 Duck94 nearshore field experiment (presented in a companion paper by Lippmann, et al.) show significant vertical structure in energy, phase, and rotation of motions at low frequencies around 0.005 Hz. Low-frequency motions are typically modeled in the surfzone with the shallow-water (depth averaged) momentum equations that do not allow for any vertical structure. Following work from the shelf tidal community (Prandle), this study shows that the observations are consistent with the depth-varying momentum equations including shear stresses induced by a bottom boundary layer described by a constant eddy viscosity ν_t and bottom friction given by a constant drag coefficient and depth-averaged velocity $c_d|\overline{W}|$. The bidirectional flow field is solved over arbitrary depth profiles varying only in the cross-shore direction $h(x)$ in the presence of a vertically uniform mean alongshore current with cross-shore shear structure $V(x)$. Analytic solutions are found to depend on ν_t, c_d, h, $\partial V/\partial x$, and the parameter $p = [i(kV - \sigma + \partial V/\partial x)/\nu_t]^{1/2} = i^{1/2}\lambda$, where σ and k are the radian frequency and alongshore wavenumber of the oscillating motion. Model behavior is explored by plotting solutions for a given parameter space as functions of the nondimensional depth $H = \lambda h$ and dimensionless friction parameter $J = \nu_t\lambda/c_d|\overline{W}|$ that combines the effects of bottom drag and vertical mixing. The behavioral changes in amplitude, phase shift, and rotational structure over the water column are qualitatively similar to those observed in the field.

1. Introduction

Since the discovery of vorticity motions in surfzone field observations in the late 1980s (Oltman-Shay et al. 1989), it has generally been assumed that the motions are uniform over depth. Initial efforts described the behavior analytically with linear stability analysis (Bowen and Holman 1989; Dodd and Thornton 1990) or numerically with nonlinear equations (e.g., Allen et al. 1996; Slinn et al. 1998; Ozkan-Haller and Kirby 1999). More recently vertical motions have been shown to be driven by variations in wave groups (Long and Özkan-Haller 2009), wave breaking patterns associated with individual waves (MacMahan et al. 2010; Clark et al. 2012; Feddersen 2014), and unforced motions associated with rip current cells (Geiman and Kirby 2013). Analyses of field data have often utilized arrays of flow meters spatially lagged in the alongshore direction (e.g., Howd et al. 1991; Noyes et al. 2004) or observations of pressure and bidirectional currents at a single location (Lippmann et al. 1999). In these studies, observations of the flow from each element of the observing array were made at a single vertical position in the water column generally near the seabed.

Recent analysis of field observations obtained at several locations in the surfzone of a naturally barred beach from a vertical array of two-component electromagnetic current meters spanning the water column show surprisingly large vertical variation in energy, phase, and rotation for low-frequency motions around 0.005 Hz. The observations are described in detail in the companion paper (Lippmann et al. 2016, hereinafter

Corresponding author address: Thomas C. Lippmann, University of New Hampshire, 24 Colovos Rd., Durham, NH 03824.
E-mail: lippmann@ccom.unh.edu

DOI: 10.1175/JPO-D-16-0015.1

Part I) and are only summarized here. At these low frequencies, most of the observed energy is associated with vorticity motions [determined using the methods of Lippmann et al. (1999)]. Energy levels in the cross-shore component of the flow decay near the bottom, seaward of the sandbar and approximately linearly over the entire water column in the trough of the bar, suggesting the influence of a bottom boundary layer. Oppositely, energy levels in the alongshore component of the flow increase near the bed seaward of the bar and are nearly uniform over depth in the trough. The coherence between each of the 8 vertically separated sensors and the sensor nearest the surface drops by as much as 70%–80% over the shallow depths of the surfzone (about 1–3 m). The phase relative to the highest sensor shifts approximately linearly over depth, with as much as 50° phase lags from top to bottom. The bottom sensors sometimes lead and sometimes lag the surface, depending on their position in the cross shore relative to the sandbar and mean alongshore current profile. Additionally, the cross-shore component of the flow near the bottom may lag the surface at the same time the alongshore component of the flow leads the surface. Rotary coefficients are generally nonzero, indicating that these low-frequency motions have rotary nature, with rotational directions that depend on the position of the sensors relative to the sandbar and alongshore current profile. The rotary coefficients are generally not uniform with depth and can change sign in the vertical. These observations reveal complex vertical behavior that the simple, shallow-water (depth uniform) models for vorticity motions do not consider.

In this paper, we present a theoretical development based on boundary layer theory following Prandle (1982) that predicts qualitatively the observed vertical behavior of low-frequency motions. The theory is described in the next section, followed by presentation of results for selected parameter values that are quantitatively similar to expected values in typical surfzone conditions.

2. Theory

Solutions to the equations of motion are obtained relative to the water surface to correspond to the vertical structure observed by Part I shown with variation relative to the uppermost sensor location. The effects of a bottom boundary layer are parameterized by a constant drag coefficient and vertical mixing dependent on a constant eddy viscosity parameter. We consider unforced solutions that include a depth uniform but horizontally varying mean alongshore current. The methodology follows that of Prandle (1982) for horizontal tidal flows (with negligible vertical velocities) on the continental shelf, except that Coriolis is neglected.

The horizontal momentum equations in the absence of surface wave forcing are given by

$$\frac{\partial}{\partial t}u' + \mathbf{u}' \cdot \nabla u' = -g\frac{\partial}{\partial x}\eta' + \frac{1}{\rho}\frac{\partial}{\partial z}F_{zx}, \quad \text{and} \tag{1}$$

$$\frac{\partial}{\partial t}v' + \mathbf{u}' \cdot \nabla v' = -g\frac{\partial}{\partial y}\eta' + \frac{1}{\rho}\frac{\partial}{\partial z}F_{zy}, \tag{2}$$

where x, y, and z are the right-handed Cartesian coordinates (with x increasing positively seaward, y aligned parallel to the shoreline, and z positive upward from the mean sea level), with corresponding horizontal velocity components $\mathbf{u}' = (u', v')$; η' is the sea surface elevation; ρ is the density of water; g is gravitational acceleration; t is the time; and ∇ is the horizontal gradient operator. The shear stresses in the x and y directions F_{zx} and F_{zy} are parameterized with a constant vertical eddy viscosity ν_t so that

$$F_{zx} = \rho\nu_t\frac{\partial}{\partial z}u', \quad \text{and} \tag{3}$$

$$F_{zy} = \rho\nu_t\frac{\partial}{\partial z}v'. \tag{4}$$

The Coriolis force is neglected in (1)–(2) because motions with typical frequencies considered here (0.05–0.001 Hz) are not greatly influenced by Coriolis.

We assume that mean cross-shore flows and pressure gradients are zero and that the total flow consists of a steady alongshore current with no vertical or alongshore variation $V(x)$, so that $u' = [\tilde{u}(x, y, z, t), \tilde{v}(x, y, z, t) + V(x)]$ with fluctuating components $\tilde{u}, \tilde{v} \ll V$ and $\eta' = \tilde{\eta}(x, y, t)$. We assume solutions that are wavelike in the alongshore direction, and with unknown cross-shore and vertical structure,

$$\tilde{u} = u(x, z)e^{i(ky-\sigma t)}, \tag{5}$$

$$\tilde{v} = v(x, z)e^{i(ky-\sigma t)}, \quad \text{and} \tag{6}$$

$$\tilde{\eta} = \eta(x)e^{i(ky-\sigma t)}, \tag{7}$$

where σ and k are the radian frequency and alongshore wavenumber of the motions. Inserting (5)–(7) into (1)–(2), using (3)–(4), and retaining only linear terms in the fluctuating velocity components, yields

$$-i\sigma u + ikVu = -g\frac{\partial\eta}{\partial x} + \nu_t\frac{\partial^2 u}{\partial z^2}, \quad \text{and} \tag{8}$$

$$-i\sigma v + ikVv + u\frac{\partial V}{\partial x} = -igk\eta + \nu_t\frac{\partial^2 v}{\partial z^2}. \tag{9}$$

If we now assume that the shear stresses are negligible at the surface and denote the spatial structure of the surface velocities with (u_o, v_o), then (8)–(9) at the surface become

$$-i\sigma u_o + ikVu_o = -g\frac{\partial \eta}{\partial x}, \quad \text{and} \tag{10}$$

$$-i\sigma v_o + ikVv_o + u_o\frac{\partial V}{\partial x} = -igk\eta. \tag{11}$$

Subtracting the surface equations from (8) to (9) eliminates the sea surface elevation and makes the velocity solutions relative to the surface value:

$$\left[i\left(\frac{kV-\sigma}{\nu_t}\right) - \frac{\partial^2}{\partial z^2}\right](u-u_o) = 0, \quad \text{and} \tag{12}$$

$$\left[i\left(\frac{kV-\sigma}{\nu_t}\right) - \frac{\partial^2}{\partial z^2}\right](v-v_o) = -\frac{1}{\nu_t}(u-u_o)\frac{\partial V}{\partial x}. \tag{13}$$

These equations are similar to those derived by Prandle (1982) for tidal flows on the continental shelf, except that the cross-shore shear of the alongshore current $\partial V/\partial x$ has replaced the role of the Coriolis force in providing a background vorticity field in the alongshore momentum equation (as in Bowen and Holman 1989). The unbalanced nature of the equations, with the cross-shore momentum equation [(12)] being homogeneous and independent of the alongshore current shear, precludes simple solution methodology (as in Prandle 1982). Solutions to (12) and (13) can be found by first doubly integrating (12) and using surface and bottom boundary conditions to find a solution for u and then using (13) and the method of undetermined coefficients (e.g., Swokowski 1979) to find v.

Since we seek solutions that reveal any rotational properties of the flow, we follow Prandle (1982) and construct the complex vector velocity w:

$$w = \tilde{u} + i\tilde{v}, \tag{14}$$

which (following Gonella 1972) can be separated into an anticlockwise (cyclonic) or positively rotating component w_+ and a clockwise (anticyclonic) or negatively rotating component w_-, such that

$$w = w_+ e^{i(ky+\sigma t)} + w_- e^{i(ky-\sigma t)}. \tag{15}$$

The rotational components are given by an amplitude $|w_+|$, $|w_-|$ and phase $|\theta_+|$, $|\theta_-|$:

$$w_+ = |w_+|e^{i\theta_+} = \frac{1}{2}[(a_1+b_2)+i(a_2-b_1)], \tag{16}$$

and

$$w_- = |w_-|e^{i\theta_-} = \frac{1}{2}[(a_1-b_2)+i(a_2+b_1)], \tag{17}$$

determined from the Fourier coefficients (a_1, b_1, a_2, b_2) of each of the velocity components u and v, whose amplitudes $|u|$, $|v|$ and phases θ_u, θ_v are given by

$$|u| = (a_1^2+b_1^2)^{1/2}, \quad \theta_u = \arctan(-b_1/a_1), \quad \text{and} \tag{18}$$

$$|v| = (a_2^2+b_2^2)^{1/2}, \quad \theta_v = \arctan(-b_2/a_2). \tag{19}$$

Using (14)–(19) provides a method for specifying a vector flow field with particular rotational properties at the surface. Solutions as a function of elevation can be decomposed into cross-spectral phases between velocity components u and v as well as the rotary coefficient R_c and ellipse orientation θ_E given by

$$R_c = \frac{-2(a_1b_2 - a_2b_1)}{(a_1^2+b_1^2)(a_2^2+b_2^2)}, \quad \text{and} \tag{20}$$

$$\tan 2\theta_E = \frac{2(a_1a_2+b_1b_2)}{(a_1^2+b_1^2)-(a_2^2+b_2^2)}. \tag{21}$$

We form a pair of governing equations, one each for the anticlockwise (denoted with + subscript) and clockwise (denoted with − subscript) rotation directions, for the vector velocity by combining (8) + $i\times$ (9) with the surface value (10) + $i\times$ (11):

$$p_+^2(w_+ - w_{o+}) - \frac{\partial^2 w_+}{\partial z^2} = -\frac{1}{\nu_t}(v-v_o)\frac{\partial V}{\partial x} \quad \text{(anticlockwise)}, \quad \text{and} \tag{22}$$

$$p_-^2(w_- - w_{o-}) - \frac{\partial^2 w_-}{\partial z^2} = -\frac{1}{\nu_t}(v-v_o)\frac{\partial V}{\partial x} \quad \text{(clockwise)}, \tag{23}$$

where the parameter p for the anticlockwise p_+ and clockwise p_- rotation is given by

$$p_+ = \left[\frac{i(kV-\sigma+\partial V/\partial x)}{\nu_t}\right]^{1/2} \quad \text{(anticlockwise)}, \quad \text{and} \tag{24}$$

$$p_- = \left[\frac{i(kV+\sigma+\partial V/\partial x)}{\nu_t}\right]^{1/2} \quad \text{(clockwise)}. \tag{25}$$

This parameter is very similar to that found by Prandle (1982), with Coriolis being replaced by $kV + \partial V/\partial x$. The solutions to (22)–(23) should reflect similar qualitative behavior as found for the tidal flow problem within the given parameter space. However, unlike in the homogenous tidal flow equations, our governing equations

for the rotational components of the vector velocity are complicated by a term that depends on the alongshore component of the flow of interest, $v - v_o$.

At the surface ($z = 0$), the shear stresses are assumed negligible ($\rho\nu_t \partial w_o/\partial z = 0$) and

$$w = w_o \quad \text{at} \quad z = 0. \tag{26}$$

At the bottom ($z = -h$, where h is the local water depth), we assume a quadratic shear stress

$$\rho\nu_t \frac{\partial w}{\partial z} = \rho c_d |\overline{W}| w \quad \text{at} \quad z = -h, \tag{27}$$

where c_d is a bottom drag coefficient, and $|\overline{W}|$ is the magnitude of the depth-averaged flow that includes both steady and unsteady components. Following Longuet-Higgins (1970), we let $|\overline{W}| = (u_{\text{orb}}^2 + V^2)^{1/2}$, where u_{orb} is the incident wave orbital velocity amplitude nominally of $O(1)\,\text{m s}^{-1}$ in the surfzone. Complex solutions to (22)–(23) for the vector velocity relative to the surface for each direction of rotation $(w/w_o)_\pm$, subject to surface and bottom boundary conditions given by (26) and (27), are found using the method of undetermined coefficients (Swokowski 1979):

$$\left(\frac{w}{w_o}\right)_\pm = \left(1 + \frac{\sinh l_\pm \frac{z}{h}}{\sinh l_\pm + j_\pm \cosh l_\pm}\right) + M_\pm \left\{ \frac{z}{h} \frac{\cosh l_\pm \frac{z}{h}}{\cosh l_\pm} - \frac{\sinh l_\pm \frac{z}{h}}{\sinh l_\pm} \left[\frac{1 + j_\pm (l_\pm^{-1} + \tanh l_\pm)}{1 + j_\pm \tanh^{-1} l_\pm} \right] \right\}, \tag{28}$$

where

$$M_\pm = \left(\frac{h \frac{\partial V}{\partial x}}{2 c_d |\tilde{W}|} \right) \left(\frac{v_o}{w_o} \right)_\pm \left(\frac{1 - e^{-l_\pm/j_\pm}}{j_\pm \tanh l_\pm} \right), \tag{29}$$

$$l_\pm = p_\pm h, \quad \text{and} \tag{30}$$

$$j_\pm = \frac{\nu_t p_\pm}{c_d |\tilde{W}|}, \tag{31}$$

and $p_\pm$ is given by (24) and (25). The first two terms in (28) arise from the homogeneous solution to (22). The remaining two terms are due to the $(v - v_o)\partial V/\partial x$ terms in (22)–(23) and depend on a number of dimensional quantities contained in (29), including h, $\partial V/\partial x$, and $|\overline{W}|$, as well as the complex surface velocities v_o and $w_o = u_o + iv_o$ that includes a phase angle for v_o, $(\theta_v)_o$, and the positive and negatively rotating components θ_{o+} and θ_{o-}.

When the mean alongshore current is absent, (29)–(31) reduce to the simplified form found by Prandle (1982) without Coriolis, a solution valid for any unforced wave motion in the surfzone including surface gravity waves. The presence of a horizontally sheared, mean, alongshore current provides a background vorticity field that supports instabilities but complicates the solution.

When $c_d = 0$, that is, the bottom drag goes away, $(w/w_o)_\pm = 1$, and there is no vertical structure. When $c_d \to \infty$, the solutions are equivalent to those found for a no-slip bottom boundary condition, and the vertical structure is largest. When c_d is finite and nonzero, the thickness of the bottom boundary layer depends also on the eddy viscosity. For large ν_t, the vertical structure becomes more uniform, compressing the bottom boundary layer to a thinner region near the bed. In our formulation, we have ignored the presence of surface shear stresses that arise from wave breaking and thus our mixing parameterized by constant eddy viscosity is solely due to bottom effects. As ν_t is dependent somewhat on the bottom drag coefficient, as represented by our quadratic shear stress at the bed described by (27), we will simply select a single value for ν_t that is grossly consistent with surfzone observations and then vary c_d to determine the effects of bottom drag on the vertical structure of the flows.

Letting $p_\pm = i^{1/2}\lambda_\pm$, where

$$\lambda_+ = \left(\frac{kV - \sigma + \partial V/\partial x}{\nu_t} \right)^{1/2}, \quad \text{and} \tag{32}$$

$$\lambda_- = \left(\frac{kV + \sigma + \partial V/\partial x}{\nu_t} \right)^{1/2}, \tag{33}$$

and $l_\pm = i^{1/2} L_\pm$ and $j_\pm = i^{1/2} J_\pm$, we can replace (30) and (31) with

$$H_\pm = \lambda_\pm h, \quad \text{and} \tag{34}$$

$$J_\pm = \frac{\nu_t \lambda_\pm}{c_d |\overline{W}|}. \tag{35}$$

The variable $H_\pm$ is similar in form to that found by Prandle (1982) for tidal flows and interpreted as a depth parameter with Ekman-like scaling. For our surfzone problem, the scaling has similar behavior but depends on the shear and magnitude of the mean alongshore current relative to the oscillation frequency; $J_\pm$ is also similar in form to that found by Prandle (1982) and represents the effects of vertical mixing (through the vertical eddy viscosity) and bottom drag (through the product of a bottom drag coefficient and depth-averaged vector velocity).

The variables $J_\pm$ and $H_\pm$ are linearly related by

$$J_\pm = \frac{\nu_t}{hc_d|\bar{W}|}H_\pm, \tag{36}$$

where the proportionality constant $\nu_t/hc_d|\bar{W}|$ is independent of rotation direction. Although a wide range of $J_\pm$ and $H_\pm$ can be specified, only those values satisfying (36) for a particular parameter set are meaningful. As values c_d for instabilities of the alongshore current are not well constrained by theory or observation, solutions described by (28) can be explored in $J_\pm$, $H_\pm$ − space for a given range of $\lambda_\pm$.

Also, note that λ_+ and λ_- are not the same for any particular wavenumber and frequency but are related by

$$\lambda_+^2 = \lambda_-^2 - \frac{2\sigma}{\nu_t}, \tag{37}$$

with σ determined from (25):

$$\sigma = \frac{\nu_t\lambda_-^2 - \partial V/\partial x}{V/c_p + 1}, \tag{38}$$

where $c_p = \sigma/k$ is the phase speed of the low-frequency motions. The complete solution for the flow field includes both positively and negatively rotating components; thus, we need to choose values for the local, mean, alongshore current V and phase speed of the wave motions of interest c_p in order to relate λ_-^2 to λ_+^2. In the results presented below, both V and c_p are given in terms of the maximum alongshore current V_o, a range of λ_-^2 are specified to correspond to typical infragravity frequencies using (38), and then the corresponding λ_+^2 are found using (37).

3. Results

The solution for the vertically varying vector flow field relative to the surface is dependent on a large parameter space that includes a factor $M_\pm$ [(29)] dependent on dimensional quantities h, $|\bar{W}|$, $\partial V/\partial x$, and the complex ratio $(v_o/w_o)_\pm$ that must be specified independently of $H_\pm$, $J_\pm$, and $\lambda_\pm$. To examine the general behavior of the solutions, we let $h = 1\,\mathrm{m}$, $\nu_t = 0.02\,\mathrm{m^2\,s^{-1}}$, $u_{\mathrm{orb}} = 1\,\mathrm{m\,s^{-1}}$, and $V_o = 1\,\mathrm{m\,s^{-1}}$, representative of surfzone conditions, and $c_p = V_o/2$ as a reasonable value for the phase speed of the vorticity wave (following Bowen and Holman 1989). In particular, the choice of eddy viscosity is consistent with model data comparisons for mean cross-shore flows (Garcez Faria et al. 2000) and is adapted without modification in the following.

Field observations at $f = 0.005\,\mathrm{Hz}$ described in the companion paper (Part I) show rotary parameters at the surface of about $R_c = 0.2$ and $\theta_E = 20°$. We thus specify the surface amplitudes and phases to give the same rotary values: $|w_o|_+ = 0.12\,\mathrm{m\,s^{-1}}$, $\theta_{o+} = 40°$, $|w_o|_- = 0.10\,\mathrm{m\,s^{-1}}$, and $\theta_{o-} = 0°$. The solutions now depend on $\partial V/\partial x$ and c_d. The general behavior of the solutions can be found by letting $\partial V/\partial x = \pm 0.025\,\mathrm{m\,s^{-1}}$, reasonable values for moderate alongshore currents in the surfzone (e.g., Thornton and Kim 1993), with the sign change representing differences on the seaward and shoreward side of the position of maximum alongshore current, and letting $c_d = 0.005$ or 0.10 for weak or strong bottom drag, respectively. Bottom drag coefficients, defined in the same way as in (27), are typically of the order of 10^{-2}–10^{-3} for mean alongshore currents (e.g., Garcez Faria et al. 1998). The values used for c_d ranging a factor of 20 are grossly representative of conditions with weak and strong bottom friction.

Solutions to (28) for the cyclonic and anticyclonic rotational components w_+ and w_- can be resolved into an amplitude $|w_\pm|/|w_{\pm o}|$ and phase shift $\theta_\pm - \theta_{o\pm}$ relative to the surface. To find solutions, λ_-^2 is specified to be −10, −5, −1, 1, 5, and 10, corresponding to $f = |\sigma/2\pi| \le 0.14\,\mathrm{Hz}$ and consistent with the range of typical frequencies of infragravity band motions observed in the field data (e.g., Oltman-Shay et al. 1989), and then $\lambda_+^2 = -3.3$, −2.1, −1.2, −0.7, 0.2, and 1.3 found from (37) and (38). Solutions for both rotational components of the flow computed with $\partial V/\partial x = -0.025\,\mathrm{s^{-1}}$ and $c_d = 0.005$ are shown in Fig. 1 as a function of relative vertical elevation in the water column z/h. As the magnitude of $\lambda_\pm^2$ decreases, the vertical amplitudes decay more strongly with depth in a progressively more linear manner, becoming approximately 70% of the surface value at the bottom for the relatively weak drag parameter used. As the magnitude of $\lambda_\pm^2$ increases, the profile becomes progressively more uniform with depth. The relative phase shifts approximately linearly over the water column with the maximum phase change at the bottom for intermediate values of $\lambda_\pm^2$. When $\lambda_\pm^2$ changes sign, the phase shift also changes sign with the bottom motion leading (negative phase shifts) the surface when $\lambda_\pm^2 < 0$.

Because of the nearly linear phase structure, the behavior of the predicted phase shifts over the vertical can be approximated with the bottom value θ_b. Contours of θ_b are shown in Fig. 2 as a function of $J_\pm^2$ and $H_\pm^2$ for $\lambda_\pm^2 < 0$ and $\lambda_\pm^2 > 0$, with $\partial V/\partial x = -0.025\,\mathrm{s^{-1}}$ and $c_d = 0.005$ (the same parameter values used in Fig. 1). For large $J_\pm^2$, the phase shifts become only a function of nondimensional depth $H_\pm^2$. As $J_\pm^2$ decreases, the phase shifts become smaller and progressively more independent of $H_\pm^2$. Because $J_\pm^2$ and $H_\pm^2$ are both proportional to $\lambda_\pm^2$, the specific locations in $J_\pm^2 - H_\pm^2$ space

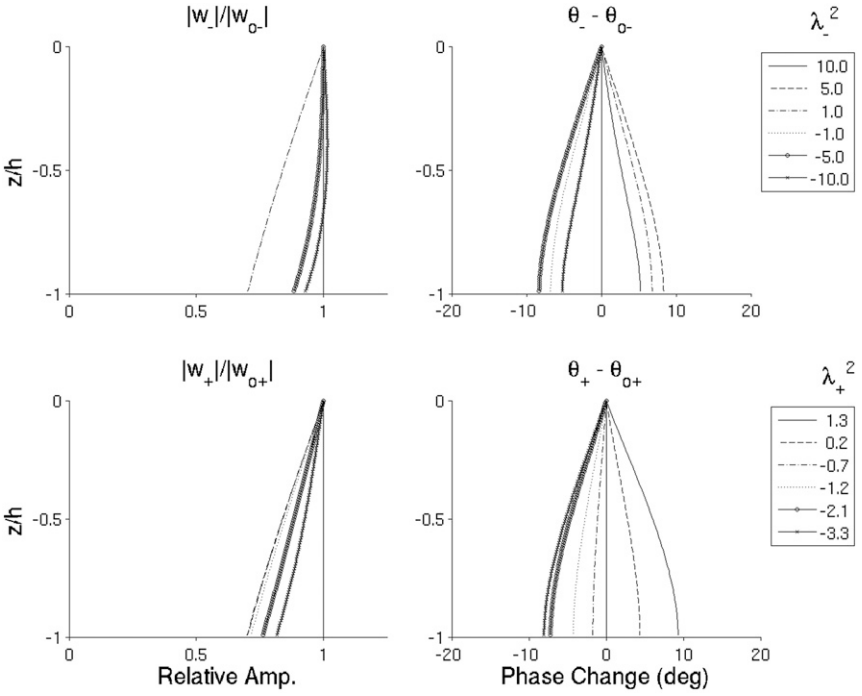

FIG. 1. Vertical profiles of (top) cyclonic and (bottom) anticyclonic velocity (left) amplitudes and (right) phase relative to the surface value as a function of relative elevation z/h for values of $\lambda^2_{\pm}$ given in the legend. Results are shown for $\partial V/\partial x = -0.025\,\mathrm{s}^{-1}$ and $c_d = 0.005$.

corresponding to any given $\lambda^2_{\pm}$ fall along a straight line with slope $\nu_t/hc_d|\bar{W}| = 2.8$, as dictated by (36). Locations where $\lambda^2_- = -10, -5, -1, 1, 5$, and 10 ($\lambda^2_{\pm} = -3.3, -2.1, -1.2, -0.7, 0.2$, and 1.3) are shown as solid circles in the upper (lower) panels of Fig. 2 and correspond to the vertical structure shown in Fig. 1. Maximum phase shifts occur for intermediate values of $\lambda^2_{\pm}$.

The vector velocity w can be determined from the rotational components using (15)–(17). The magnitude $|w/w_o|$ and phase $\theta - \theta_o$, relative to the surface value, is shown in Fig. 3 as a function of z/h for the rotational components presented in Fig. 1, with $\partial V/\partial x = -0.025\,\mathrm{s}^{-1}$, $c_d = 0.005$, and $\lambda^2_- = -10, -5, -1, 1, 5$, and 10. For the relatively weak bottom drag specified, the amplitudes decay to about 70% of their surface value for small λ^2_-, with maximum bottom phase shifts of about $-10°$, with the sign of the phase shift changing as the sign of λ^2_- changes, similar to the behavior of the rotational components presented earlier (as expected). Contours of θ_b for the vector velocity are shown in Fig. 2 as a function of $|J^2_-|$ and $|H^2_-|$ for $\lambda^2_- < 0$ and J^2_- and H^2_- for $\lambda^2_- > 0$. The phase behavior is nearly symmetric for positive and negative λ^2_- with maximum phase shifts occurring for small H^2_-. Locations where $\lambda^2_- = -10, -5, -1, 1, 5$, and 10 are shown as solid circles and correspond to the vertical structure shown in Fig. 3.

The effect on bottom friction is evaluated by increasing the drag to $c_d = 0.10$. Contours of θ_b are shown in Fig. 4 for $\partial V/\partial x = -0.025\,\mathrm{s}^{-1}$ and $\lambda^2_- = -10, -5, -1, 1, 5$, and 10, the same parameters used in Figs. 2 and 3. Vertical phase shifts are much larger for the case with large bottom drag, with maximum phase change of about 45° occurring at intermediate values of λ^2_-. The slope of the line $\nu_t/hc_d|\bar{W}| = 0.14$ corresponding to values of λ^2_- has decreased inversely proportional to the factor of 20 increase in c_d.

The effect of changing signs in the shear of the alongshore current, as occurs when moving spatially from seaward to shoreward of the maximum alongshore current, is shown in Fig. 5. Contours of θ_b are shown for the same range of λ^2_- and $c_d = 0.10$ as in Fig. 4, but now $\partial V/\partial x = 0.025\,\mathrm{s}^{-1}$ has opposite sign. In this case, the phase shifts have decreased by about 2/3 with maximum value of about 32° again occurring at intermediate values of λ^2_-.

We can compute the Cartesian velocities u and v from the solutions for the rotating components of the vector velocity using (16)–(19). In this case, we select a range of frequencies, $f = \sigma/2\pi = 0.001, 0.005, 0.01$, and 0.02 Hz, and then compute corresponding parameters λ^2_- and λ^2_+ from (37) and (38). Vertical variation in amplitude $|u/u_o|$ and $|v/v_o|$ and phase $\theta_u - (\theta_u)_o$ and $\theta_v - (\theta_v)_o$ as a function of z/h are shown in Fig. 6 with

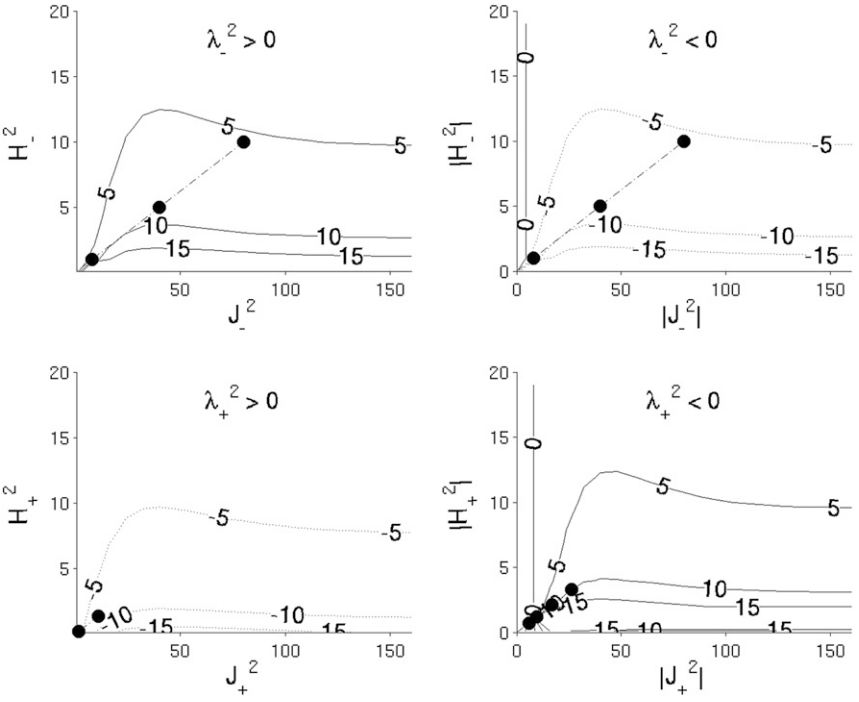

FIG. 2. Contours of θ_b for the (top) cyclonic and (bottom) anticyclonic rotational components as a function of $|J_{\pm}^2|$ and $|H_{\pm}^2|$ for (left) $\lambda_{\pm}^2 > 0$ and (right) $\lambda_{\pm}^2 < 0$. Results are shown for $\partial V/\partial x = -0.025\,\mathrm{s}^{-1}$ and $c_d = 0.005$. Solid circles in the upper (lower) panels indicate values for $\lambda_{-}^2 = -10, -5, -1, 1, 5$, and 10 ($\lambda_{+}^2 = -3.3, -2.1, -1.2, -0.7, 0.2$, and 1.3), corresponding to those used in Fig. 1 showing the vertical variation in amplitude and phase.

$\partial V/\partial x = -0.025\,\mathrm{s}^{-1}$ and intermediate drag given by $c_d = 0.010$. Relative cross-shore velocity amplitudes $|u/u_o|$ attenuate with depth for all frequencies in a nearly linear fashion, with increasing attenuation with decreasing frequency, consistent with a thicker bottom boundary layer for longer-period motions. Cross-shore phase structure $\theta_u - (\theta_u)_o$ has maximum phase shift at the bottom occurring at intermediate frequencies, in this case around $f = 0.005$ Hz. In contrast, alongshore velocities show a complex structure in which relative amplitudes $|v/v_o|$ decay at the lowest frequencies (around $f = 0.001$ Hz), are nearly uniform with depth at intermediate frequencies (around $f = 0.005$ Hz), and then increase at higher frequencies ($f > 0.005$ Hz) with subsurface maximum in the lower half of the water column. Phase shifts are nearly linear with depth and with a sign change between $f = 0.001$ and $f = 0.005$ Hz.

Phase shifts relative to the surface vary with frequency and are different in magnitude and sign for u and v, with larger negative phase shifts for v approaching 22° at the bottom for intermediate frequencies. The phase behavior is complex, with u leading and v lagging the surface. The sign and magnitude of the phase shift is determined by the direction of rotation selected for the surface vector velocity amplitudes and phases for the clockwise and counterclockwise rotating components. By switching the dominant rotational amplitude or altering the relative phases of the rotational components, the major axis of the ellipse changes orientation; thus, the u and v phase shifts relative to the surface can also be modified and can change sign depending on the amplitudes and phases of the rotary velocity components.

The effect of $\partial V/\partial x$ on the behavior of u and v is examined by plotting the bottom phase shift for u and v, $(\theta_u)_b$ and $(\theta_v)_b$, respectively, as a function of frequency for $\partial V/\partial x = \pm 0.025\,\mathrm{s}^{-1}$. Results are shown in Fig. 7 for intermediate bottom drag $c_d = 0.010$. At higher frequencies up to 0.05 Hz, $(\theta_u)_b$ is about 2° and $(\theta_v)_b$ is about 11°, regardless of the sign of $\partial V/\partial x$; $(\theta_u)_b$ reaches a negative maximum around $f = 0.005$ Hz and is larger by about a factor of 4 for negative (−11°) than for positive (−2.5°) $\partial V/\partial x$. When $\partial V/\partial x$ is positive, $(\theta_v)_b$ is roughly constant, ranging between 7° and 13°. On the other hand, when $\partial V/\partial x$ is negative, $(\theta_v)_b$ reaches a positive maximum (24°) around $f = 0.012$ Hz and then rapidly decreases at lower frequencies, becoming negative when $f < 0.005$ Hz. The phase structure in either u or v can thus have opposite sign across the mean alongshore current

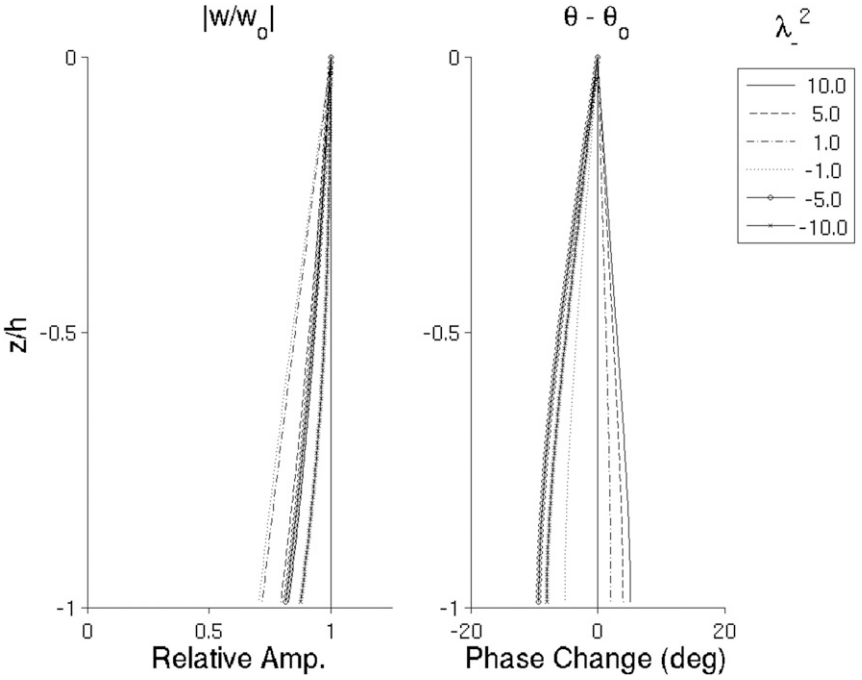

FIG. 3. Vertical profiles of vector velocity (left) amplitudes and (right) phase relative to the surface value as a function of relative elevation z/h for values of λ^2_- given in the legend. Results are shown for $\partial V/\partial x = -0.025\,\mathrm{s}^{-1}$ and $c_d = 0.005$.

profile, with bottom velocities leading and lagging the surface on the seaward and shoreward side of V_o, particularly for v, which has much stronger dependence on the sign of $\partial V/\partial x$ than does u.

The effect of large and small bottom friction on the behavior of u and v is examined by plotting $(\theta_u)_b$ and $(\theta_v)_b$ for $\partial V/\partial x = -0.025\,\mathrm{s}^{-1}$ as a function of frequency for $c_d = 0.10$ and 0.005 (Fig. 8). For weak bottom friction, phase changes for the cross-shore flows are weak, with $(\theta_u)_b$ ranging $+2°$ to $-8°$ over the infragravity frequency band but are relatively stronger for alongshore flows with $(\theta_v)_b$ reaching a positive maximum (17°) around $f = 0.01$ Hz and changing sign at the lowest frequencies. Phase structure as a function of frequency is more pronounced for higher drag coefficients, with $(\theta_u)_b$ going from 0° at $f = 0.001$ Hz to a negative maximum of $-35°$ around $f = 0.008$ Hz and gradually down to about $-5°$ at higher frequencies. Phase changes for v are high and nearly constant (about 28°–30°) for $f > 0.01$ Hz but decrease rapidly to a large negative value ($-37°$) at $f = 0.001$ Hz. Figures 7 and 8 show that, in general, $(\theta_u)_b$ tends be negative (i.e., leading the surface), whereas $(\theta_v)_b$ can be large positive ($f > 0.01$ Hz) or large negative ($f < 0.005$ Hz) for the same $\partial V/\partial x$ or c_d.

The rotary parameters R_c and θ_E can be computed as a function of frequency from (20) and (21) using the Fourier coefficients for u and v given by (18) and (19). The vertical variation of R_c and θ_E is shown in Fig. 9 for $f = 0.001, 0.005, 0.01$, and 0.02 Hz, with $\partial V/\partial x = -0.025\,\mathrm{s}^{-1}$ and intermediate bottom drag $c_d = 0.010$. The surface values of R_c and θ_E are determined from the input conditions specified earlier. The results show that the current orientation rotates farther down into the water column with θ_E at the bottom increasing about 10° relative to the surface for $f > 0.001$ Hz and decreasing by about 5° for $f = 0.001$ Hz. The results also show that R_c has strong vertical variation, and for $f > 0.001$ Hz, R_c changes sign in about the midwater column, indicating that the sense of rotational motion is different at the surface (clockwise in the example) than at the bottom (counterclockwise).

The effect of $\partial V/\partial x$ on R_c and θ_E is shown in Fig. 10 as a function of frequency for intermediate bottom drag $c_d = 0.01$ and $\partial V/\partial x = \pm 0.025\,\mathrm{s}^{-1}$. Crossing the location of V_o, for example, when moving from positive to negative $\partial V/\partial x$, can rotate the current orientation, as indicated by $\Delta\theta_E = (\theta_E)_b - (\theta_E)_o$ shown in the lower panel of Fig. 10. As well, a vertical sign change in the sense of rotation can occur at particular intermediate frequencies, $0.005\,\mathrm{Hz} < f < 0.02\,\mathrm{Hz}$ in this case, as shown by $(R_c)_b$ in the upper panel of Fig. 10. The effect of bottom friction on R_c and θ_E is shown in Fig. 11 as a function of frequency for $\partial V/\partial x = -0.025\,\mathrm{s}^{-1}$ and $c_d = 0.005$ and 0.10. Changes in current orientation are much larger

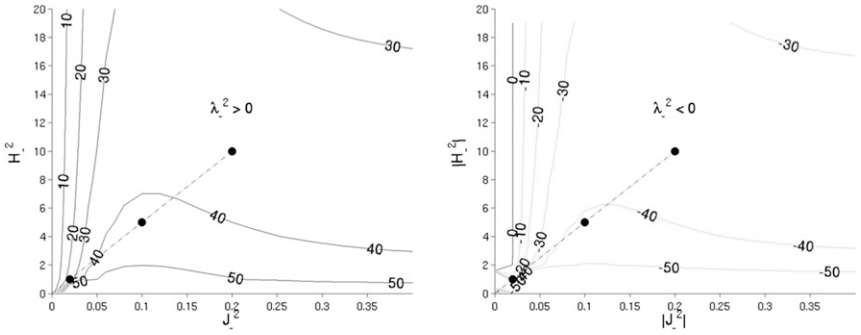

FIG. 4. Contours of θ_b for the vector velocity as a function of $|J_-^2|$ and $|H_-^2|$ for (left) $\lambda_-^2 > 0$ and (right) $\lambda_-^2 < 0$. Results are shown for $\partial V/\partial x = -0.025\,\mathrm{s}^{-1}$ and $c_d = 0.10$. Solid circles indicate values for $\lambda_-^2 = -10, -5, -1, 1, 5$, and 10 corresponding to those used in Fig. 3 showing the vertical variation in amplitude and phase.

for strong bottom drag, with rotations increasing by about 20° over most of the infragravity band for larger c_d. Vertical variations in rotation also increase with increasing drag, with R_c changing sign in the vertical for $f > 0.001$ Hz.

4. Discussion

The boundary layer theory developed here, following Prandle (1982) for tidal motions on the continental shelf, qualitatively describes the complex vertical amplitude, phase, and rotational structure of vortical motions observed in the field. The parameter space is large and dimensional quantities need to be assigned. Values for h, $\partial V/\partial x$, V_o, and c_p used are quantitatively consistent with values observed in the field. Values for ν_t and c_d are consistent with those found in model data comparisons for mean flows. Although the local values of h and $V(x)$ are measured, $\partial V/\partial x$ can only be roughly estimated. In addition, while the assumptions of vertically constant alongshore current and eddy viscosity are necessary to allow analytic solutions, they are clearly substantial approximations. Including vertical structure (particularly in V) is likely to further emphasize the complexity of the vertical structure. However, the theory yields results that suggest the modeled equations are appropriate. Considering the complex behavior in vertical structure observed and modeled, numerical models examining quantitative vorticity motion behavior and dynamical consequences for surfzone processes should consider the vertical structure.

In the absence of a mean alongshore current, the solutions collapse to those found by Prandle (1982) with the exception that Coriolis is not relevant to nearshore motions with typically much higher frequency. Inclusion of mean alongshore currents allows for a background vorticity field that supports instabilities. The solutions are also valid for surface gravity waves in the presence of a mean alongshore flow, and they suggest that edge and leaky waves will also exhibit complex vertical structure, particularly for the longer periods in which the boundary layer has time to develop.

Putrevu and Svendsen (1995) examined the vertical structure of infragravity waves in the surfzone. In their work, they consider only cross-shore currents and include wave forcing by shortwave radiation stresses lumped together with mean pressure contributions (setup). They solve the inhomogeneous x-momentum

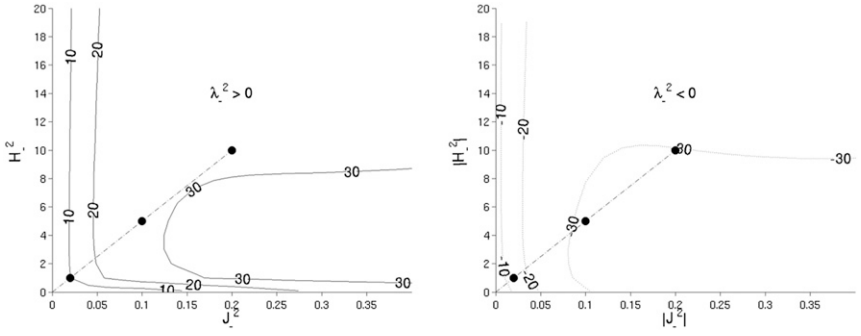

FIG. 5. As in Fig. 4, but for $\partial V/\partial x = 0.025\,\mathrm{s}^{-1}$.

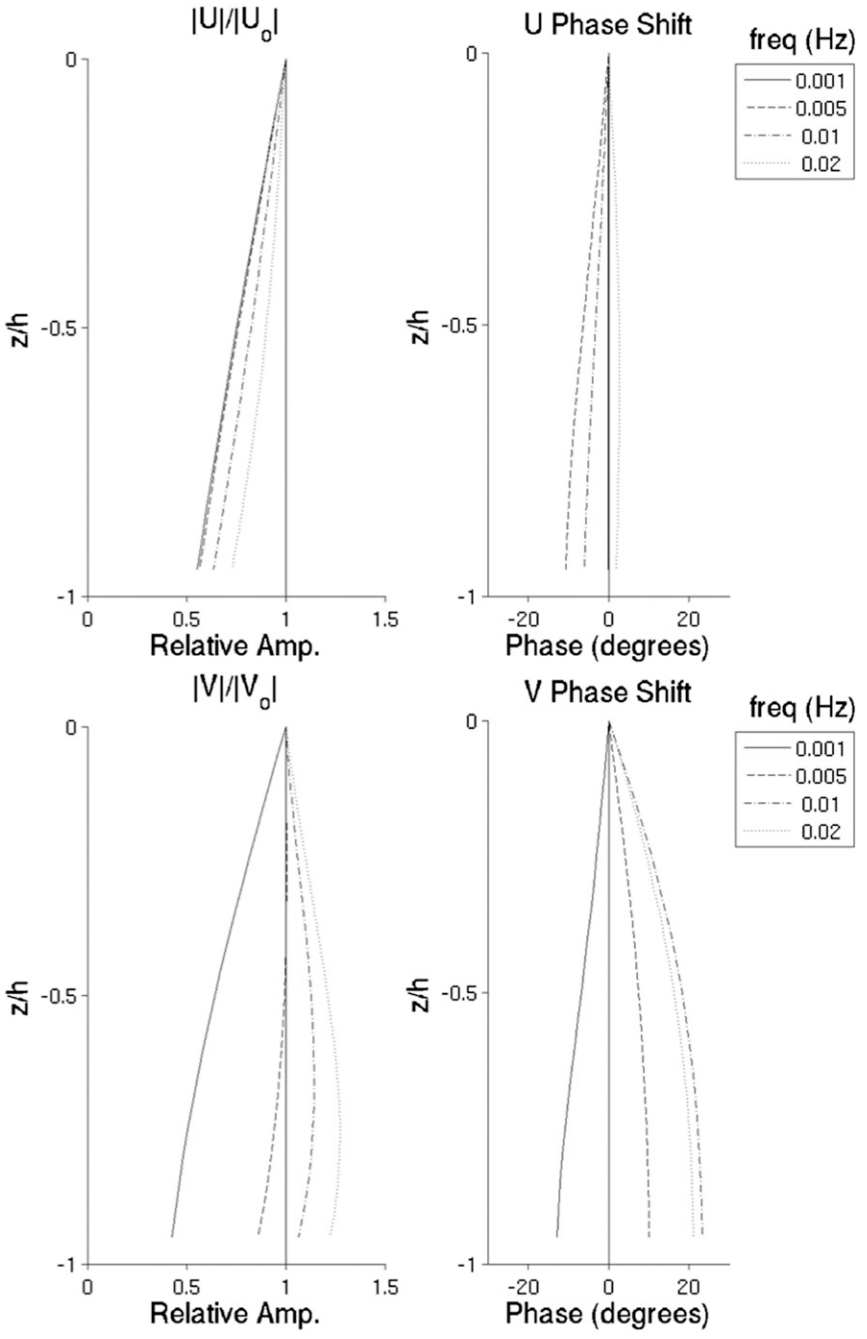

FIG. 6. Vertical profiles of horizontal velocity component (top) u and (bottom) v and (left) magnitude and (right) phase relative to the surface value as a function of relative elevation z/h for values of frequencies (Hz) given in the legend. Results are shown for $\partial V/\partial x = -0.025\,\mathrm{s}^{-1}$ and $c_d = 0.010$.

equation subject to a bottom boundary condition for bed shear stress similar to ours as well as a surface shear stress determined by (and phase locked to) the short-wave forcing. They parameterize the forcing and keep track of the phase relationship between the group forcing and the response, thus their solutions are representative of forced waves that do not freely propagate beyond the group structure of the prescribed forcing and thus are quite different in nature than our situation for free waves. They conclude that forced waves have strong vertical variation in amplitude and phase but that free infragravity waves do not. This is in

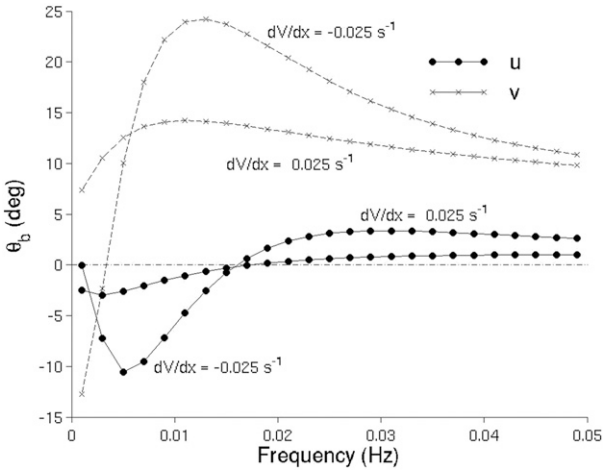

FIG. 7. Effect of $\partial V/\partial x$ on relative bottom phase shift θ_b plotted as a function of wave frequency (Hz) for u (solid dots) and v (cross marks) with $c_d = 0.01$. Results are shown for $\partial V/\partial x = \pm -0.025\,\mathrm{s}^{-1}$.

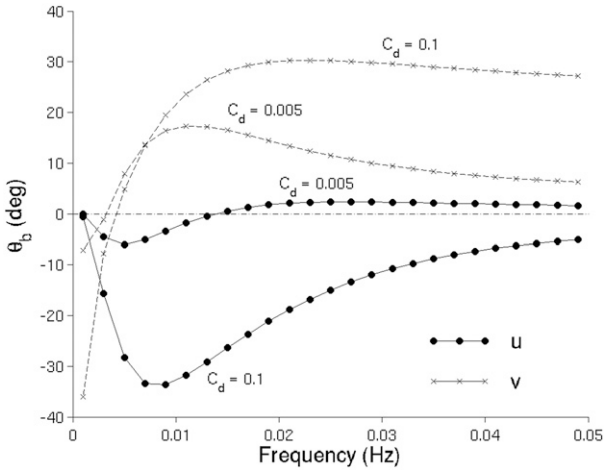

FIG. 8. Effect of c_d on relative bottom phase shift θ_b plotted as a function of wave frequency (Hz) for u (solid dots) and v (cross marks) for $\partial V/\partial x = -0.025\,\mathrm{s}^{-1}$. Results are shown for $c_d = 0.1, 0.005$.

contrast to the results described here where we have considered only unforced motion at infragravity frequencies.

Interpretation of surface gravity waves is complicated by the cross-shore nodal structure that for a broad distribution of energy across all wavenumbers depends on the edge wave mode mix. In general, results here [as well as by Prandle (1982)] suggest that all free infragravity motions should exhibit vertical structure, particularly at lower frequencies. Further examination of surface gravity waves that includes theoretical representation of their cross-shore structure (e.g., on a planar beach profile) is the subject of ongoing research.

The results show that the sign of the vertical phase change depends on the sign of λ^2. When λ^2 becomes negative, an additional i is introduced into the parameter $p_\pm$ [(24) and (25)]. The additional i effectively changes the direction of rotation because the velocity profile structure given by (28) depends on exponentials of the form $\exp(\pm p_\pm z)$, similar to tidal flows as pointed out by Prandle (1982); λ^2 can be positive or negative depending on the relative magnitudes of kV, $\partial V/\partial x$, and σ and thus sign changes can occur when moving across the surfzone and passing the location of V_o (i.e., as the sign of $\partial V/\partial x$ changes). In this work, we have only considered V to be uniform over depth. In natural surfzones, V has vertical structure, particularly in the lower half of the water column (Garcez Faria et al. 1998). If the vertical variation in V is strong enough, and assuming the phase speed of the motions $c_p = \sigma/k$ is constant with depth, a local rotational change can occur over the vertical independent of $\partial V/\partial x$. That is, V can be greater than c_p at the surface but less than c_p near the bottom, thereby introducing a rotational change over the water column. A similar situation exists if we consider cross-shore mean flows that also have significant vertical variation (e.g., Garcez Faria et al. 2000). Inclusion of vertically varying mean flows significantly complicates the equations, and solutions are not readily derived and therefore are not considered herein.

It should be noted that our results are computed with typical values of current speeds, cross-shore current shear, and bottom drag in order to characterize the overall properties of the oscillatory motions. However, our solutions vary only as a function of elevation z and do not consider that the instantaneous current structure and parameter space that may vary as a function of cross-shore location x. This spatial variation might be significant over cross-shore scales associated with vorticity motions, a problem that Prandle (1982) did not have to consider for tides. However, the vorticity motion orbital excursion is relatively small compared to typical surfzone widths and profile variations (that scale with sandbar positions and beach slope), suggesting that the cross-shore scaling may not be an issue. We have not neglected any differentiations with respect to x (other than the nonlinear advective terms) but have ignored terms that arise from cross-shore profile variations (typically present in nature). How these nonlinear or bottom slope terms modify our results is not established here but is expected to be of higher order.

Depth-integrated values of cross-shore and alongshore velocities are solutions to the vorticity equation and satisfy any constraint, including continuity (e.g., Bowen and Holman 1989). Zhao et al. (2003)

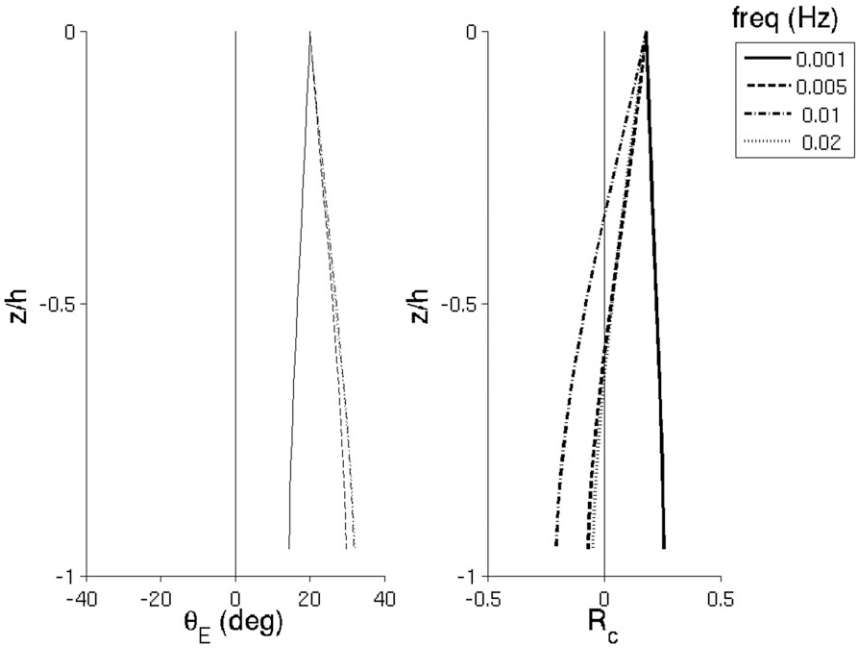

FIG. 9. Vertical profiles of rotary parameters (left) θ_E and (right) R_c as a function of relative elevation z/h for values of wave frequency (Hz) given in the legend. Results are shown for $\partial V/\partial x = -0.025\,\mathrm{s}^{-1}$ and $c_d = 0.010$.

developed a numerical model that separates depth uniform from vertically varying flow and uses a quasi-3D approach by specifying an analytic formulation for the departure from a local, depth-uniform momentum balance (following Putrevu and Svendsen 1999). Their leading-order solution has quadratic form determined by shortwave (radiation stresses) and local momentum fluxes, bottom drag formulation, and balancing a vertically integrated volume flux. Their solution for the vertical variation depends on the nature of the wave forcing, whereas our vertically varying flows depend on characteristics of the existing flow field specified at the surface a priori and a bottom drag coefficient that modifies the structure. Furthermore, in this work, we have not explicitly derived or specified theoretical solutions for the surface values, u_o and v_o, nor derived any dispersion relation. If these surface values are known, or say estimated from a depth-integrated model, then our application of the vertical structure could be applied to the solutions under the assumption of a given dispersion relation [e.g., $c_p = \sigma/k = V_o/2$ after Bowen and Holman (1989)] without specifying the nature of the wave radiation stress forcing or vertical moment balances, a potential limitation of our approach in quantitative comparisons to field data. Finally, although Zhao et al. (2003) compare their quasi-3D model to a 2D depth-integrated model, no comparisons have been made to fully 3D models that we are aware of and thus how fully three-dimensional effects impact the vertical structure is not known and cannot be compared to our results at this time.

In this work, following Bowen and Holman (1989) who assumed a rigid-lid approach to modeling shear instabilities of the longshore current, we are assuming that the vertical velocities of the vortical motions are negligible compared to the horizontal velocities at frequencies of interest (about 0.005 Hz). In general, vertical velocities of low-frequency vortical motions in the nearshore are believed be quite small, of $O(0.001)\,\mathrm{m\,s}^{-1}$, and difficult to observe. If those small values for vertical velocities are taken as typical, a depth scaling of $O(1)$ m, and our assumed eddy viscosity of $0.02\,\mathrm{m}^2\,\mathrm{s}^{-1}$, the inertial terms for vertical velocity components are more than an order of magnitude less than the viscous terms.

Our results show that observations of the vertical structure of low-frequency motions in the nearshore (described in the companion paper) are qualitatively reproduced with the boundary layer model using the observed surface values for rotational properties and reasonable values for the magnitude of alongshore currents at this beach ($1\,\mathrm{m\,s}^{-1}$), phase speeds for dominant vorticity wave propagation (approximated as half the maximum longshore current), water depths (1 m), wave orbital velocities ($1\,\mathrm{m\,s}^{-1}$), and eddy mixing coefficients in the nearshore ($0.02\,\mathrm{m}^2\,\mathrm{s}^{-1}$; after

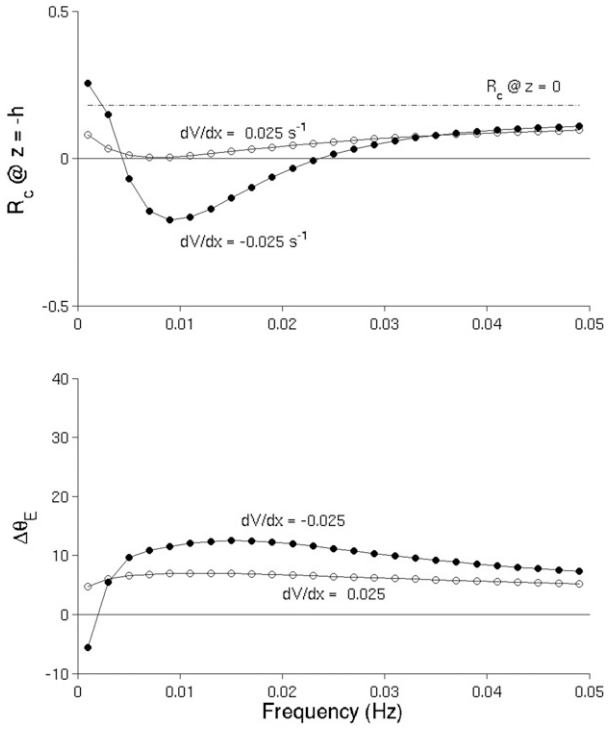

FIG. 10. (top) Effect of $\partial V/\partial x$ on change in R_c and (bottom) relative phase shift in ellipse orientation $\Delta\theta_E = (\theta_E)_b - (\theta_E)_o$, plotted as a function of wave frequency for $c_d = 0.01$. The surface value for R_c is shown as the dashed–dotted line in the top panel. Results are shown for $\partial V/\partial x = -0.025\,\mathrm{s}^{-1}$ (solid dots) and $\partial V/\partial x = 0.025\,\mathrm{s}^{-1}$ (open circles).

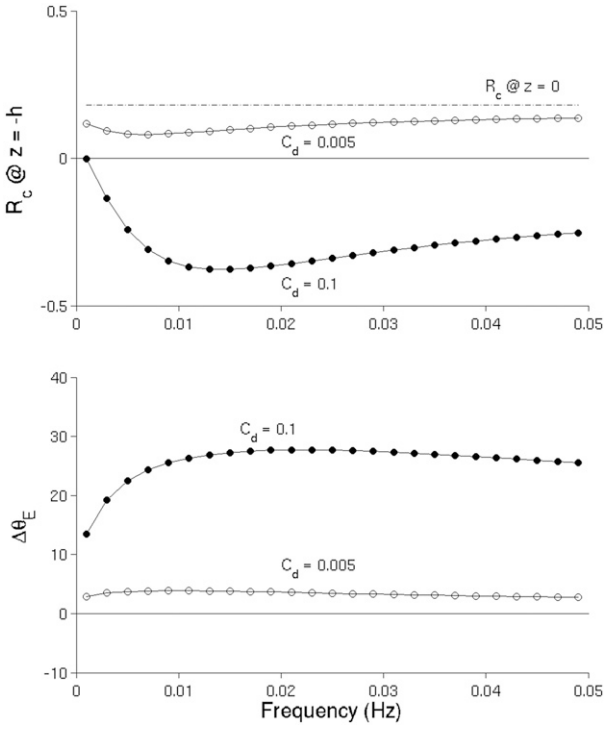

FIG. 11. (top) Effect of c_d on change in R_c and (bottom) relative phase shift in ellipse orientation $\Delta\theta_E = (\theta_E)_b - (\theta_E)_o$, plotted as a function of wave frequency for $\partial V/\partial x = -0.025\,\mathrm{s}^{-1}$. The surface value for R_c is shown as the dashed–dotted line in the top panel. Results are shown for $c_d = 0.1$ (solid dots) and $c_d = 0.005$ (open dots).

Garcez Faria et al. 2000). The behavior of the model thus depends on the magnitude of bottom drag coefficients and the cross-shore shear of the mean alongshore current (including changes in sign). Under a reasonable range of bottom drag and current shears, the behavior of the vertical variation in current direction and rotational properties are reproduced. In particular, the vertical variation in amplitude and phase (relative to the surface value) of the cross-shore and alongshore components of the flows at the bottom and the rotational components (rotary coefficient and ellipse orientation), including midwater column sign changes.

5. Conclusions

Analytic solutions to the viscous, linearized, unforced horizontal momentum equations are found that predict a complex vertical structure associated with low-frequency oscillatory motions in the nearshore in the presence of a horizontally sheared, depth-uniform, mean, alongshore current $V(x)$. The vertical distribution of horizontal shear stresses are parameterized by a depth-uniform eddy viscosity ν_t and a quadratic bottom stress formulation that includes the product of a constant drag coefficient c_d and the depth-averaged vector flow field $|\bar{W}|$. The development follows closely that for tidal flows on the continental shelf (Prandle 1982) without inclusion of Coriolis. The inclusion of V in the equations results in an inhomogeneous equation for the vector velocity that is solved using the method of undetermined coefficients.

Solutions are shown to depend on a dense but manageable set of variables, including the water depth h, horizontal shear of the mean alongshore current $\partial V/\partial x$, and the parameter $p = [i(kV \pm \sigma + \partial V/\partial x)/\nu_t]^{1/2} = i^{1/2}\lambda$. By letting $h = 1$ m and $\nu_t = 0.02\,\mathrm{m}^2\,\mathrm{s}^{-1}$, representative of typical surfzone conditions, model behavior is examined in terms of λ^2, c_d, and $\partial V/\partial x$, and by forming the nondimensional depth $H = \lambda h$ and dimensionless friction parameter $J = \nu_t\lambda/c_d|\overline{W}|$ that combines the effects of bottom drag and vertical mixing.

Amplitudes relative to the surface are found to vary over depth, consistent with typical boundary layer flow that extends over the entire water column. The vertical phase structure is complex. Phases relative to the surface

vary approximately linearly over depth and can have up to 45° phase shifts at the bottom depending on the parameter space examined. The sign of the phase shift depends on the sign of λ^2, with negative λ^2 generally corresponding to bottom velocities leading the surface. Interestingly, the sign of the phase shift for cross-shore flows can be opposite that of alongshore flows at the same position in the surfzone, indicating that bottom cross-shore flows can lag the surface while at the same time alongshore flows lead.

The bottom phase shift also varies as a function of frequency and depends on the strength of the bottom drag c_d and the mean current shear $\partial V/\partial x$. At higher frequencies, phase shifts are generally smaller than about 20°. Maximum phase shifts occur for cross-shore components of the velocity at low frequencies around 10^{-2}–10^{-3} Hz, but for alongshore flows the maximum phase shift can become large at the lowest frequencies and can change sign depending on the sign of the current shear. In general, phase shifts are higher when the bottom drag increases and can also increase (or decrease) as $\partial V/\partial x$ changes sign.

Solutions are found for rotational properties of the flow by forming the vector velocity. A surface condition is specified by amplitudes and phases for clockwise and counterclockwise rotating components that define the rotary coefficient and ellipse orientation. The solutions predict a turning of the flows with depth by as much as 20° over the water column for the parameter space examined. Rotary coefficients are not uniform over depth and can change sign, indicating that the sense of rotation near the surface can be opposite to that near the bottom.

The complex vertical structure in amplitude, phase, and rotation is qualitatively consistent with new analyses of field observations (presented in Part I) from a vertical stack of two component current meters obtained at the 1994 Duck94 nearshore field experiment. Solutions are valid for a range of frequencies spanning the infragravity band, but analysis focuses on the lowest-frequency band around 0.005 Hz in which nearly all the motions are associated with vorticity motions. The results show complex vertical behavior necessarily absent in the commonly used shallow-water (depth averaged) solutions.

Acknowledgments. We thank the anonymous reviewers whose comments greatly improved the paper. T. C. L. was funded by the Office of Naval Research, Coastal Geosciences program, under Grants N000140210238 and N000141410557. A. J. B. was supported by the Natural Science and Engineering Research Council, Canada.

REFERENCES

Allen, J. S., P. A. Newberger, and R. A. Holman, 1996: Nonlinear shear instabilities of alongshore currents on plane beaches. *J. Fluid Mech.*, **310**, 181–213, doi:10.1017/S0022112096001772.

Bowen, A. J., and R. A. Holman, 1989: Shear instabilities of the mean longshore current: 1. Theory. *J. Geophys. Res.*, **94**, 18 023–18 030, doi:10.1029/JC094iC12p18023.

Clark, D. B., S. Elgar, and B. Raubenheimer, 2012: Vorticity generation by short-crested wave breaking. *Geophys. Res. Lett.*, **39**, L24604, doi:10.1029/2012GL054034.

Dodd, N., and E. B. Thornton, 1990: Growth and energetics of shear waves in the nearshore. *J. Geophys. Res.*, **95**, 16 075–16 083, doi:10.1029/JC095iC09p16075.

Feddersen, F., 2014: The generation of surfzone eddies in a strong alongshore current. *J. Phys. Oceanogr.*, **44**, 600–617, doi:10.1175/JPO-D-13-051.1.

Garcez Faria, A. F., E. B. Thornton, T. P. Stanton, C. V. Soares, and T. C. Lippmann, 1998: Vertical profiles of longshore currents and related bed shear stress and bottom roughness. *J. Geophys. Res.*, **103**, 3217–3232, doi:10.1029/97JC02265.

——, ——, T. C. Lippmann, and T. P. Stanton, 2000: Undertow over a barred beach. *J. Geophys. Res.*, **105**, 16 999–17 010, doi:10.1029/2000JC900084.

Geiman, J. D., and J. T. Kirby, 2013: Unforced oscillation of rip-current vortex cells. *J. Phys. Oceanogr.*, **43**, 477–497, doi:10.1175/JPO-D-11-0164.1.

Gonella, J., 1972: A rotary-component method for analyzing meteorological and oceanographic vector time series. *Deep-Sea Res. Oceanogr. Abstr.*, **19**, 833–846, doi:10.1016/0011-7471(72)90002-2.

Howd, P. A., J. Oltman-Shay, and R. A. Holman, 1991: Wave variance partitioning in the trough of a barred beach. *J. Geophys. Res.*, **96**, 12 781–12 795, doi:10.1029/91JC00434.

Lippmann, T. C., T. H. C. Herbers, and E. B. Thornton, 1999: Gravity and shear wave contributions to nearshore infragravity motions. *J. Phys. Oceanogr.*, **29**, 231–239, doi:10.1175/1520-0485(1999)029<0231:GASWCT>2.0.CO;2.

——, E. B. Thornton, and T. P. Stanton, 2016: The vertical structure of low frequency wave motions in the nearshore. Part I: Observations. *J. Phys. Oceanogr.*, **46**, 3695–3711, doi:10.1175/JPO-D-16-0014.

Long, J. W., and H. T. Özkan-Haller, 2009: Low-frequency characteristics of wave group–forced vortices. *J. Geophys. Res.*, **114**, C08004, doi:10.1029/2008JC004894.

Longuet-Higgins, M. J., 1970: Longshore currents generated by obliquely incident sea waves: 1. *J. Geophys. Res.*, **75**, 6778–6789, doi:10.1029/JC075i033p06778.

MacMahan, J. H., A. J. H. M. Reniers, and E. B. Thornton, 2010: Vortical surf zone velocity fluctuations with O(10) min period. *J. Geophys. Res.*, **115**, C06007, doi:10.1029/2009JC005383.

Noyes, T. J., R. T. Guza, S. Elgar, and T. H. C. Herbers, 2004: Field observations of shear waves in the surf zone. *J. Geophys. Res.*, **109**, C01031, doi:10.1029/2002JC001761.

Oltman-Shay, J., P. A. Howd, and W. A. Birkemeier, 1989: Shear instabilities of the mean longshore current: 2. Field observations. *J. Geophys. Res.*, **94**, 18 031–18 042, doi:10.1029/JC094iC12p18031.

Ozkan-Haller, H. T., and J. T. Kirby, 1999: Nonlinear evolution of shear instabilities of the longshore current: A comparison of observations and computations. *J. Geophys. Res.*, **104**, 25 953–25 984, doi:10.1029/1999JC900104.

Prandle, D., 1982: The vertical structure of tidal currents and other oscillatory flows. *Cont. Shelf Res.*, **1**, 191–207, doi:10.1016/0278-4343(82)90004-8.

Putrevu, U., and I. A. Svendsen, 1995: Infragravity velocity profiles in the surf zone. *J. Geophys. Res.*, **100**, 16 131–16 142, doi:10.1029/95JC01284.

——, and ——, 1999: Three-dimensional dispersion of momentum in wave-induced nearshore currents. *Eur. J. Mech.*, **18**, 409–427, doi:10.1016/S0997-7546(99)80038-7.

Slinn, D. N., J. S. Allen, P. A. Newberger, and R. A. Holman, 1998: Nonlinear shear instabilities of alongshore currents over barred beaches. *J. Geophys. Res.*, **103**, 18 357–18 379, doi:10.1029/98JC01111.

Swokowski, E. W., 1979: *Calculus with Analytic Geometry*. Taylor and Francis, 1085 pp.

Thornton, E. B., and C. S. Kim, 1993: Longshore current and wave height modulation at tidal frequency inside the surf zone. *J. Geophys. Res.*, **98**, 16 509–16 519, doi:10.1029/93JC01440.

Zhao, Q., I. A. Svendsen, and K. Haas, 2003: Three-dimensional effects in shear waves. *J. Geophys. Res.*, **108**, 3270, doi:10.1029/2002JC001306.